Nanoscale

PAPER

View Article Online
View Journal | View Issue

Cite this: *Nanoscale*, 2014, **6**, 1195

A dual enzyme functionalized nanostructured thulium oxide based interface for biomedical application†

Jay Singh,[ac] Appan Roychoudhury,[be] Manish Srivastava,[b] Pratima R. Solanki,[d] Dong Won Lee,[a] Seung Hee Lee*[a] and B. D. Malhotra*[bef]

Received 20th September 2013
Accepted 28th October 2013

DOI: 10.1039/c3nr05043b

www.rsc.org/nanoscale

In this paper, we present results of the studies related to fabrication of a rare earth metal oxide based efficient biosensor using an interface based on hydrothermally prepared nanostructured thulium oxide (n-Tm_2O_3). A colloidal solution of prepared nanorods has been electrophoretically deposited (EPD) onto an indium-tin-oxide (ITO) glass substrate. The n-Tm_2O_3 nanorods are found to provide improved sensing characteristics to the electrode interface in terms of electroactive surface area, diffusion coefficient, charge transfer rate constant and electron transfer kinetics. The structural and morphological studies of n-Tm_2O_3 nanorods have been carried out by X-ray diffraction (XRD), scanning electron microscopy (SEM), transmission electron microscopy (TEM), X-ray photoelectron spectroscopy (XPS) and Fourier transform infrared (FTIR) spectroscopic techniques. This interfacial platform has been used for fabrication of a total cholesterol biosensor by immobilizing cholesterol esterase (ChEt) and cholesterol oxidase (ChOx) onto a Tm_2O_3 nanostructured surface. The results of response studies of the fabricated ChEt–ChOx/n-Tm_2O_3/ITO bioelectrode show a broad linear range of 8–400 mg dL^{-1}, detection limit of 19.78 mg (dL $cm^{-2})^{-1}$, and high sensitivity of 0.9245 μA (mg per dL $cm^{-2})^{-1}$ with a response time of 40 s. Further, this bioelectrode has been utilized for estimation of total cholesterol with negligible interference (3%) from analytes present in human serum samples. The utilization of this n-Tm_2O_3 modified electrode for enzyme-based biosensor analysis offers an efficient strategy and a novel interface for application of the rare earth metal oxide materials in the field of electrochemical sensors and bioelectronic devices.

Introduction

The rare earth (RE) metal oxides have recently aroused much interest from researchers actively engaged in different scientific disciplines including materials science, bioscience and nanotechnology due to their interesting properties and potential applications.[1–7] The RE metal oxides have been found to display high surface basicity, fast oxygen ion mobility, efficient charge transfer ability and interesting catalytic properties.[8] These properties have been predicted to be useful for their application as bioprobes, drug discovery, medical diagnostics, genetic analysis, flow cytometry and sensing. Among the various RE metal oxides, thulium oxide (Tm_2O_3) is being used in X-ray equipment,[9] as an active agent of phosphors,[10] as a control material of atomic reactors,[11] as a luminescent material,[12] and in medical[13] and semiconductor applications.[14] Thulium oxide has also been found to be a promising material for fabricating a sensing membrane of an ion-sensitive field-effect transistor (ISFET) and as an electrochemical impedance spectroscopy (EIS) based sensing device due to its high dielectric constant (~13), large energy band gap (>5 eV), and high chemical and thermal stability.[15] Sheng *et al.* found that a terbium

[a]*Department of BIN Fusion Technology, Department of Polymer-Nano Science and Technology, Chonbuk National University, Jeonju, Jeonbuk 561-756, Korea. E-mail: lsh1@jbnu.ac.kr; Fax: +82-63-270-2341; Tel: +82-063-270-2343*

[b]*Department of Biotechnology, Delhi Technological University, Shahbad Daulatpur, Main Bawana Road, Delhi 110042, India. E-mail: bansi.malhotra@gmail.com; Fax: +91-11-27871023; Tel: +91-11-27294668*

[c]*Department of Applied Chemistry, Delhi Technological University, Shahbad Daulatpur, Main Bawana Road, Delhi 110042, India*

[d]*Special Centre for Nano Sciences, Jawaharlal Nehru University, New Delhi 110067, India*

[e]*Department of Science & Technology, Centre on Biomolecular Electronics, Biomedical Instrumentation Section, Materials Physics & Engineering Division, CSIR-National Physical Laboratory, Dr. K. S. Krishnan Marg, New Delhi 110012, India*

[f]*Centre for Nano Bioengineering & SpinTronics, Chungnam National University, 220 Gubg-Dong, Yuseong-Gu, Daejeon 305-764, Korea*

† Electronic supplementary information (ESI) available: XPS spectra of n-Tm_2O_3, differential pulse voltammograms, magnitude of potential difference as a function of scan rate (10–100 mV s^{-1}), effect of working potential, amount of enzyme used for immobilization, amount of enzyme loading, effect of interferents, response time, effect of temperature, determination of cholesterol in serum samples and photometric enzyme activity studies. See DOI: 10.1039/c3nr05043b

hexacyanoferrate (TbHCF) modified electrode has a good electrocatalytic activity towards ascorbic acid.[16] Meng *et al.* designed a novel biosensor based on TmHCF nanoparticles entrapped in a chitosan film on the electrode surface for glucose detection.[17] Li *et al.* fabricated a glucose oxidase immobilized nafion-Tm_2O_3 film and achieved direct electron transfer with an apparent heterogeneous electron transfer rate constant (K_s) of 3.27 ± 0.43 s^{-1}.[18] Tolstopyatova *et al.* investigated the catalytic properties of Tm_2O_3 for dehydrogenation and dehydration of alcohols ($C_nH_{2n+1}OH$ series) and the dehydrogenation of tetralin.[19] Additionally, Tm_2O_3 nanoparticles synthesized by the hydrothermal method indicate an excellent biocompatibility and provide a friendly microenvironment for electron transfer between hemoglobin (Hb) and a Hb immobilized nafion-Tm_2O_3 film electrode.[20]

Total cholesterol estimation is considered to be very important for patients suffering from heart disease, atherosclerosis, hypertension, coronary artery disease, cerebral thrombosis, arteriosclerosis, lipid metabolism dysfunction and other clinical disorders that require continuous monitoring of total cholesterol in a biological sample.[21,22] It is known that 70% of cholesterol exists in ester form and 30% in free form in a blood sample.[23] Traditionally, cholesterol is measured using non-enzymatic spectrometry *via* production of colored substances such as cholestapolyenes and cholestapolyene carbonium ions. This method suffers from poor specificity, instability of the color reagents, standardization difficulties and corrosive nature of the reagent used.[24] Therefore, it is essential to develop a fast, sensitive and selective technique to measure cholesterol in biological samples. In this context, amperometric cholesterol biosensors have been considered to be efficient devices due to good selectivity, sensitivity, fast response and for reproducible data.[25] The development of electrochemical cholesterol biosensors has received much interest because of ease of preparation, high sensitivity, good specificity and fast response time. Moreover, the electrochemical biosensing involves a simple procedure and it does not require any expensive equipment. Due to simplicity, rapidness and cost-effectiveness, a cholesterol biosensor can be developed using ChEt, ChOx and peroxidase immobilized onto various membranes or matrices.[26–30] With this in view, nanostructured materials with different sizes and shapes can be utilized as substrates for the immobilization of desired enzymes.[31]

Enzyme immobilization has recently attracted much interest. However, the availability of a desired enzyme is frequently inadequate due to instability, high cost and limited possibility of economic recoveries of these biocatalysts.[32] In this context, one-dimensional (1D) metal oxide nanorods perhaps offer excellent prospects for interfacing biological recognition events with electronic signal transducer for fabrication of amperometric biosensors and bioelectronic devices.[33] This is because these small dimensional structures can be used for efficient transport of electrons. The large surface area coupled with the possibility of tunable electron transport of these interesting nanostructured materials due to quantum confinement is known to play a significant role in the operation of the desired biosensor.[34] Liu *et al.* studied the electron transfer and photothermal effect of a glucose biosensor using gold nanorods. They found that with decreasing particle size, the response current increases gradually resulting in increased enzyme loading that in turn leads to enhanced current response.[35,36]

The preparation and application of n-Tm_2O_3 nanorods towards the fabrication of an electrochemical cholesterol biosensor is considerably important. For synthesis of nanorods, a low temperature environment (200 °C) hydrothermal route of synthesis can perhaps be used to obtain well-dispersed and homogeneous distribution of nanorods.[20,34] Many processes have been proposed for deposition of thin films of nanomaterials on a conductive electrode surface for the fabrication of electrochemical bio-transducers. Among these, an electrophoretic deposition (EPD) technique is known to yield a uniform, dense and porous film with the advantages of reduced processing time and simple experimental design. In particular, as a wet process, EPD provides easy control of thickness and morphology of the deposited film by tailoring various parameters such as deposition time, applied potential, *etc.*[37,38]

We report results of the studies related to the preparation of Tm_2O_3 nanorods *via* a hydrothermal method for development of a total cholesterol biosensor. Besides this, attempts have been made to investigate electrochemistry of the interface, resulting from immobilization of ChEt and ChOx onto an n-Tm_2O_3 modified electrode electrophoretically deposited onto an indium-tin-oxide (ITO) glass substrate.

Results

Structural and morphological studies

Fig. 1A and B show schematic of the preparation of n-Tm_2O_3 nanorods (random orientation) and the biochemical reaction mechanism of the immobilized ChOx and ChEt to cholesterol oleate, respectively. Fig. 2A shows X-ray diffraction pattern of the hydrothermally synthesized n-Tm_2O_3. The observed diffraction peaks corresponding to the planes (222), (400), (411), (332), (431), (440), (611) and (622) are consistent with the standard XRD data for the Tm_2O_3 phase (JCPDS file no. 10-0350). Moreover, the presence of sharp XRD peaks suggest crystalline nature of the synthesized n-Tm_2O_3. No other phases are seen revealing the phase purity of the n-Tm_2O_3 sample.

Fig. 2B and C show TEM images of the as-synthesized n-Tm_2O_3 nanoparticles indicating a rod-like structure. A quantitative analysis of size distribution of n-Tm_2O_3 nanorods obtained through the TEM studies is shown in Fig. 2D & E. As shown in the figure, the histogram (length/diameter of nanorods) fitted by Gaussian function reveals that the synthesized nanorods have an average length of ~610 nm and a diameter of ~70 nm.

Fourier transform infrared spectroscopy

FT-IR spectra (in the range of 400–4000 cm^{-1}) of the n-Tm_2O_3, n-Tm_2O_3/ITO electrode and ChEt–ChOx/n-Tm_2O_3/ITO bioelectrodes are shown in Fig. 3A. The FT-IR spectrum of n-Tm_2O_3 powder (curve a) exhibits weak bands at 3428 cm^{-1} corresponding to O–H stretching due to physically adsorbed water. The small peaks seen at 1510 and 1383 cm^{-1}

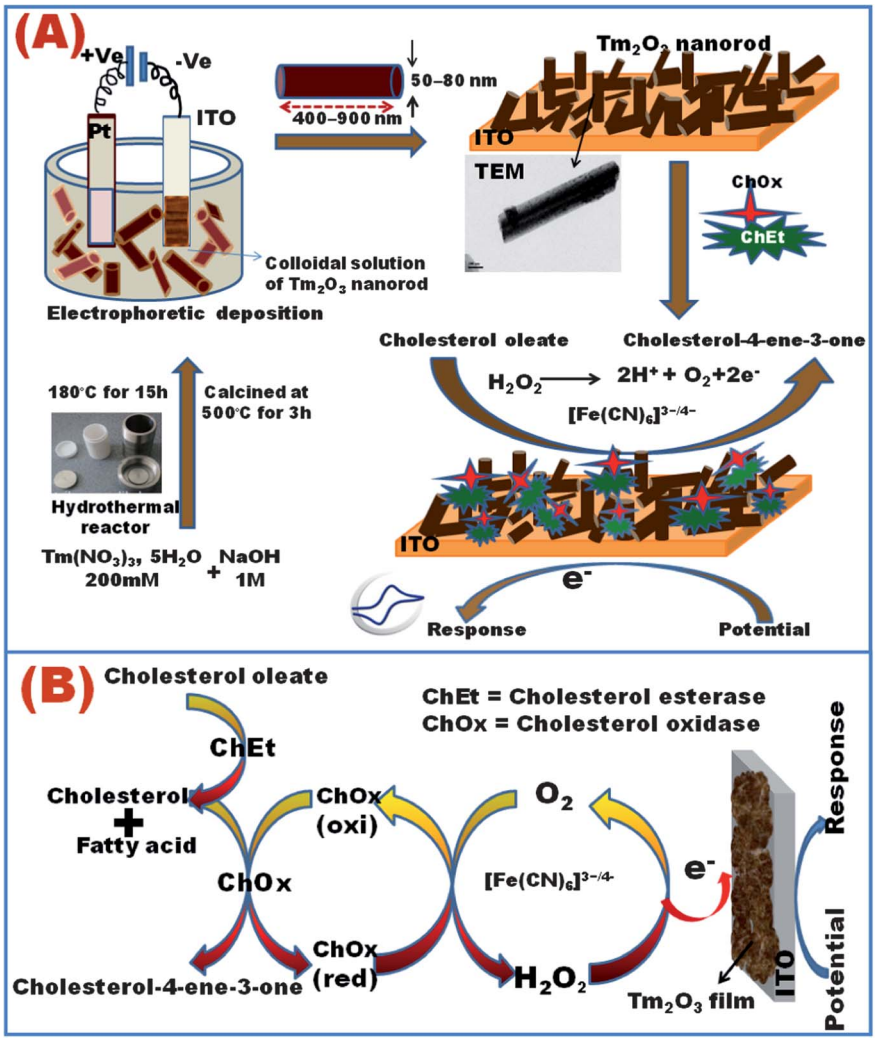

Fig. 1 (A & B) Schematic illustration for the preparation of n-Tm_2O_3 and the biochemical reaction mechanism of ChOx and ChEt towards cholesterol oleate.

are due to adsorbed carbonate and chlorate moieties. The two strong absorption bands of n-Tm_2O_3 nanorods appear at 575 and 517 cm^{-1} pertaining to the stretching vibration mode of the metal oxide (M–O) bond. After deposition of n-Tm_2O_3 onto the ITO coated glass surface (curve b), the broadening of the metal oxide bond (M–O) is observed due to electrostatic interactions between the surface functionalized ITO coated glass electrode and metal oxide. However, after immobilization of the enzymes (ChOx and ChEt) onto the n-Tm_2O_3/ITO electrode surface, the characteristic peaks seen at 1580 cm^{-1} and 1181 cm^{-1} are assigned to C–O stretching of the amide bands in protein revealing the presence of enzymes at the ChEt–ChOx/n-Tm_2O_3/ITO bioelectrode (curve c) *via* electrostatic interactions.[30,39] The peak at 1367 cm^{-1} corresponds to the asymmetric and symmetric bending vibrations of enzymes (ChOx and ChEt) CH_3 groups.[40] Fig. 3B and C show scanning electron microscopy images of n-Tm_2O_3 nanorods. The randomly distributed n-Tm_2O_3 nanorods exhibit a rod-like spindle morphology with a high degree of cluster formation.

X-ray photoelectron spectroscopy

The composition of the synthesized n-Tm_2O_3 has been examined by XPS measurements. The wide range XPS survey spectrum of the synthesized sample exhibits no impurities except for carbon as the reference. The deconvoluted spectra of Tm 4d and O 1s are shown in Fig. S1 in the ESI.† The position of Tm 4d and O 1s peaks shows the binding energies to be 176 eV and 530.4 eV suggesting the formation of Tm_2O_3. The O 1s centered around 530 eV can be ascribed to the metal oxide bond.[41] The Tm and O ratio determined using the measured peak intensities (area) of Tm 4f and O 1s and the atomic sensitivity factor found to be 1 : 1.6 indicating that Tm in the film is totally oxidized.

Cyclic voltammetric studies

Fig. 4A shows a typical cyclic voltammetric (CV) curve obtained for the bare ITO, n-Tm_2O_3/ITO electrode and ChEt–ChOx/n-Tm_2O_3/ITO bioelectrode, respectively, in PBS (50 mM, pH 6.0, 0.9% NaCl) containing $[Fe(CN)_6]^{3-/4-}$ (5 mM) at a 30 mV s^{-1} scan rate in the potential range of −0.3 V to 0.7 V. The CV of

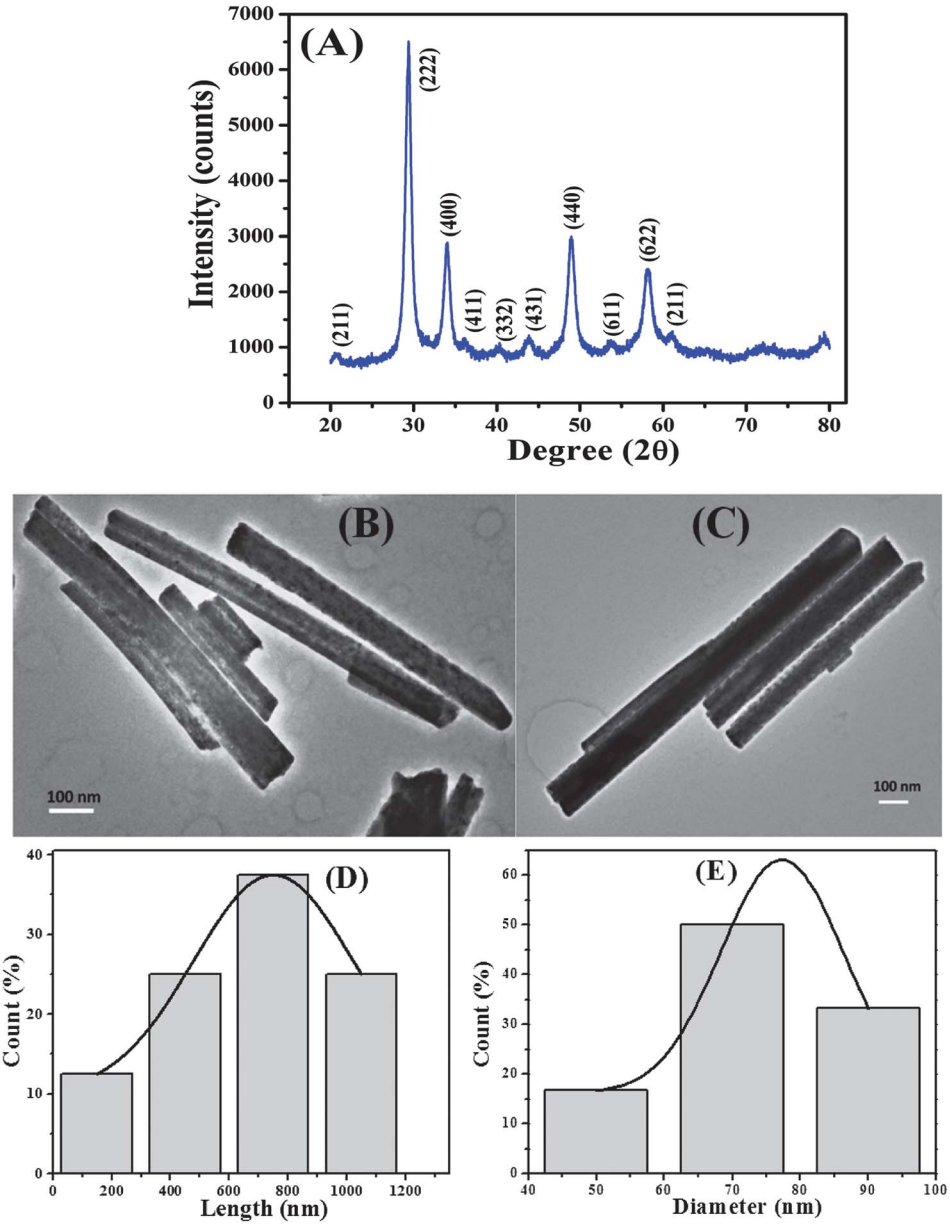

Fig. 2 (A) X-ray diffraction pattern. (B & C) TEM micrograph of the Tm_2O_3 nanorods and (D & E) histograms and Gaussian fits for length (nm) and diameter (nm) of synthesized n-Tm_2O_3 nanorods respectively.

bare ITO (curve a) exhibits well-defined electrochemical characteristics with a couple of redox peaks for the $[Fe(CN)_6]^{3-/4-}$ mediator and shows an oxidation peak current (I_{pa}) of 0.18 mA. After EPD of n-Tm_2O_3 nanoparticles onto bare ITO (curve b), the magnitude of the oxidation peak current increases to 0.27 mA due to the cationic nature of n-Tm_2O_3 nanoparticles on the ITO surface. The electrocatalytic ability, increased surface area and surface energy of n-Tm_2O_3 nanorods help to facilitate the electron transfer. Moreover, the magnitude of the oxidation peak current further increases after immobilization of ChEt and ChOx enzymes (1 : 1) onto the n-Tm_2O_3/ITO electrode, resulting in an increased peak current with oxidation (I_{pa}) and reduction (I_{pc}) peaks at 0.33 mA and −0.32 mA, respectively (curve c). This may perhaps be due to the fact that the n-Tm_2O_3/ITO electrode provides an electroactive surface area that promotes electron conduction pathways and enhanced electron movement between the active site of enzymes and the electrode and the availability of non-binding sites onto enzymes and the n-Tm_2O_3/ITO electrode, results in accelerated electron transfer in the interface. The results of the differential pulse voltammetry (DPV) studies (see Fig. S2 in the ESI†) reveal similar electrochemical behaviour of the redox potential.

To investigate the interfacial kinetics of the ChEt–ChOx/n-Tm_2O_3/ITO bioelectrode surface, CV studies have been conducted as a function of scan rate varying from 10 to 100 mV s^{-1} (Fig. 4B). It can be seen that magnitudes of both anodic (I_{pa}) and cathodic (I_{pc}) peak currents increase linearly with square root of scan rate ($\upsilon^{1/2}$) (Fig. 4C). With increasing scan rate the oxidation peak shifts towards more positive potential and similarly reduction peak shifts towards more negative potential,

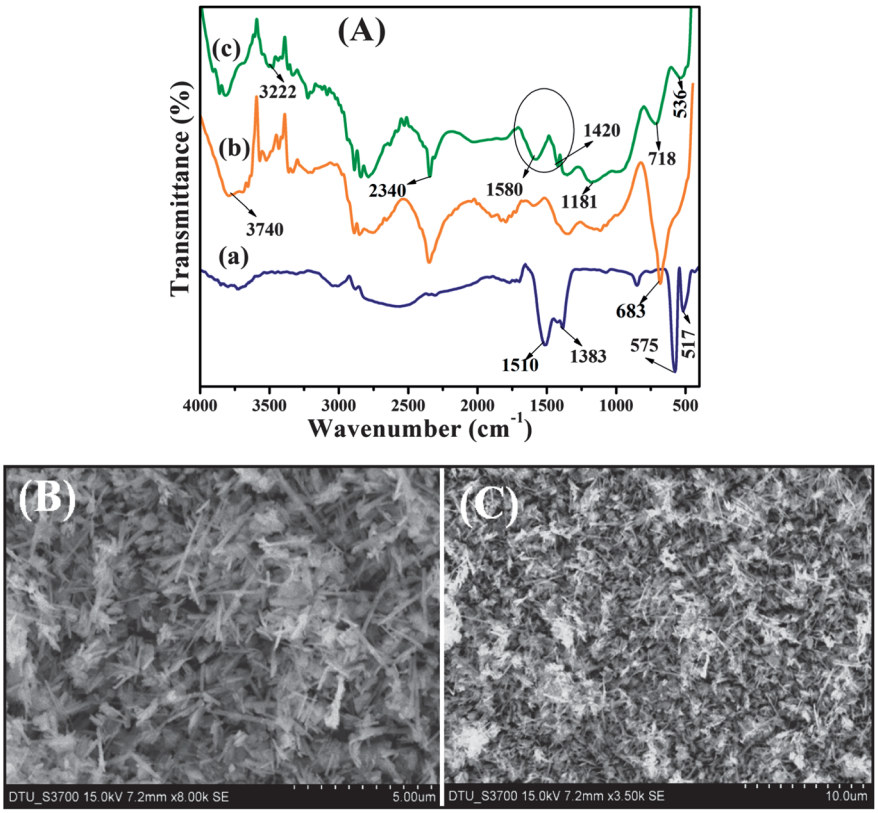

Fig. 3 (A) FTIR spectra of (a) Tm_2O_3 nanorod powder, (b) n-Tm_2O_3/ITO film, and (c) ChEt–ChOx/n-Tm_2O_3/ITO bioelectrode. (B & C) SEM image of n-Tm_2O_3 nanorods at different magnifications.

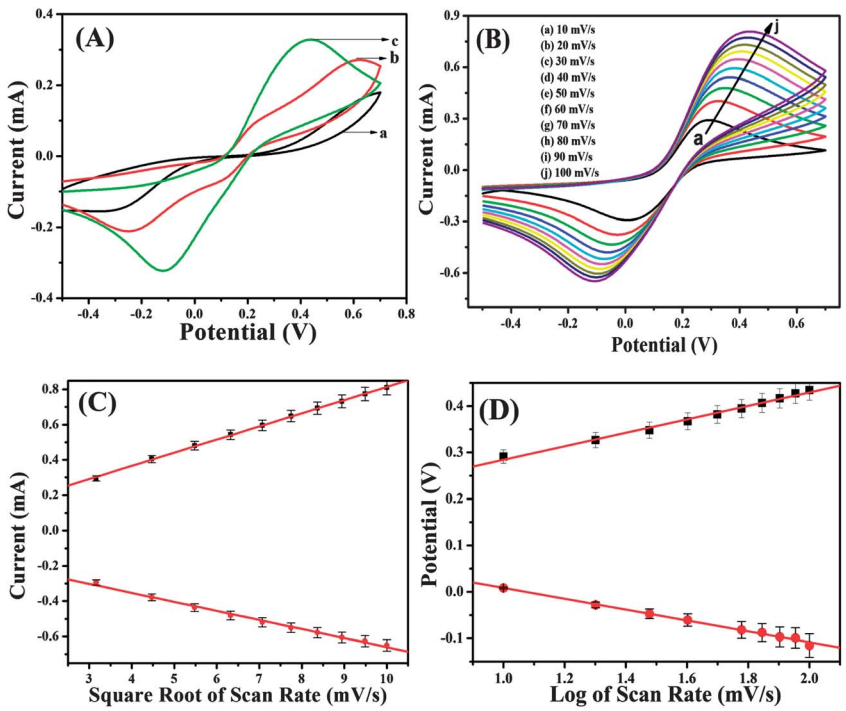

Fig. 4 (A) Cyclic voltammogram of a bare ITO electrode (a), the n-Tm_2O_3/ITO electrode (b) and the ChEt–ChOx/n-Tm_2O_3/ITO bioelectrode (c). (B) CV curve of the ChEt–ChOx/n-Tm_2O_3/ITO bioelectrode using an increasing scan rate of 10 to 100 mV s^{-1}. (C) The magnitude of the current *vs.* potential difference as a function of square root of scan rate (10–100 mV s^{-1}) and (D) peak potential shows that the linear relationship with logarithmic function of scan rate was measured in PBS (50 mM, pH 6.0, 0.9% NaCl) containing $[Fe(CN)_6]^{3-/4-}$ (5 mM) at a 30 mV s^{-1} scan rate in the potential range of −0.3 V to 0.7 V.

indicating that the redox process is quasi-reversible. The peak potential also shows a linear relationship with logarithmic function of scan rate (Fig. 4D). The value of electron transfer co-efficient (α), for n number of electrons, has been calculated from two straight lines with a slope equal to $2.3RT/(1-\alpha)nF$ for the anodic peak and $-2.3RT/\alpha nF$ for the cathodic peak, using Laviron's equations.[42] The electron transfer co-efficient (α) for the ChEt–ChOx/n-Tm_2O_3/ITO bioelectrode has been found to be 0.1453.

The change in value of the charge transfer rate constant (K_s) of the electrode due to surface modification has been calculated by following[43] eqn (1).

$$K_s = mnFv/RT \quad (1)$$

where m is the peak-to-peak separation (V), F is the Faraday constant (96 485 C mol^{-1}), v is the scan rate (30 mV s^{-1}), n is the number of transferred electrons (2), R is the gas constant (8.314 J mol^{-1} K^{-1}) and T is the room temperature (25 °C). The K_s value of the n-Tm_2O_3/ITO electrode and the ChEt–ChOx/n-Tm_2O_3/ITO bioelectrode has been found to be 2.076 s^{-1} and 1.315 s^{-1} respectively. The increased K_s value at the surface of the n-Tm_2O_3/ITO electrode clearly indicates that both the electronic structure and surface physicochemistry of the Tm_2O_3 nanorods contribute to increased electron transfer arising from high catalytic behaviour of Tm_2O_3 nanoparticles. However the fabricated bioelectrode exhibits faster electron transfer kinetics. This may perhaps be due to oriented immobilization of the biomolecules on the n-Tm_2O_3/ITO electrode surface that provides an easier path for the transfer of electrons from the redox species to the electrode and *vice versa*.[44] The anodic (E_{pa}) and cathodic (E_{pc}) peak potentials and potential peak shift ($\Delta E_p = E_{pa} - E_{pc}$) exhibit a linear relationship (see Fig. S3 in the ESI†) with scan rate. These results reveal that the biochemical reaction at the electrode is a diffusion controlled process. The diffusion co-efficient value (D) for free diffusion of $[Fe(CN)_6^{3-/4-}]$ from electrolyte solution to the corresponding electrode surface has been calculated using the Randles–Sevcik equation.[45]

$$I_p = (2.69 \times 10^5)n^{3/2}AD^{1/2}Cv^{1/2} \quad (2)$$

where I_p is the peak current of the corresponding electrode (I_{pa} anodic and I_{pc} cathodic), n is the number of electrons involved or electron stoichiometry (1), A is the surface area of the bioelectrode (0.25 cm^2), D is the diffusion co-efficient, C is the surface concentration in mol (5 mM) and v is the scan rate (30 mV s^{-1}). It can be seen from Table 1 that the ChEt–ChOx/n-Tm_2O_3/ITO bioelectrode shows a higher D value (3.19×10^{-5} mol cm^{-2}) as compared to that of the n-Tm_2O_3/ITO electrode (2.17×10^{-5} mol cm^{-2}). The electroactive surface area (A_e) of the ChEt–ChOx/n-Tm_2O_3/ITO bioelectrode is determined from the calculated diffusion co-efficient and the Randles–Sevcik equation.[46]

$$A_e = S/(2.99 \times 10^5)n^{3/2}CD^{1/2} \quad (3)$$

where S is the slope of the straight line obtained from the graph of I_p *versus* $v^{1/2}$. The A_e value of the ChEt–ChOx/n-Tm_2O_3/ITO bioelectrode has been found to be 0.88 mm^2.

It can be seen that the peak height varies directly with the sweep rate (with linear regression coefficient 0.982), indicating improved electrocatalytic behaviour. For a surface controlled process, the surface concentration of ionic species of the corresponding electrode can be estimated using the Brown-Anson model[22] based on eqn (4)

$$I_p = n^2F^2\gamma Av/4RT \quad (4)$$

where n is the number of electrons transferred (1), F is the Faraday constant (96 485 C mol^{-1}), γ is the surface concentration of ionic species of the electrode (mol cm^{-2}), A is the surface area of the electrode (0.25 cm^2), v is the scan rate (30 mV s^{-1}), R is the gas constant (8.314 J mol^{-1} K^{-1}) and T is the room temperature (25 °C). The surface concentration of the ChEt–ChOx/n-Tm_2O_3/ITO bioelectrode (4.69×10^{-11} mol cm^{-2}) is higher than that of the n-Tm_2O_3/ITO (3.88×10^{-11} mol cm^{-2}) electrode. This may perhaps be due to high surface coverage of the immobilized enzymes onto the n-Tm_2O_3/ITO electrode. Table 1 shows the values of interfacial kinetic parameters of the corresponding electrodes during the surface-controlled process.

Electrochemical impedance spectroscopy (EIS) studies

The Nyquist plot (Fig. 5A) demonstrates that semi-circle of the bare ITO electrode ($R_{ct} = 2.462$ kΩ, curve a), a characteristic of a diffusion limiting step of the electrochemical process, decreases for the n-Tm_2O_3/ITO electrode ($R_{ct} = 1.748$ kΩ, curve b). The decreased value of R_{ct} is due to the high electrocatalytic efficiency and large surface area of the Tm_2O_3 nanorods. These results suggest that the electron transfer or conductive pathway at the n-Tm_2O_3/ITO interface is more efficient between the electrolyte and the electrode surface. However, after immobilization of the enzymes (ChOx and ChEt molecules) onto the n-Tm_2O_3/ITO electrode surface, the value of ($R_{ct} = 0.922$ kΩ, curve c) decreases due to reduced negative charge on the surface by enzyme coverage and the presence of amino groups in the enzymes.[47,48] The decrease in R_{CT} value may also be attributed to the presence of a large number of polarizable groups such as amine, *etc.* in the enzymes (ChOx and ChEt) molecules onto the surface that are perhaps polarized at the open circuit potential. The polarization may result in positive charge on the surface that enhances mobility of the redox probe $[Fe(CN)_6]^{3-/4-}$ to the electrode leading to the decrease of the charge transfer resistance.[2] Furthermore, ChEt and ChOx rearrange their structures and provide a better micro-environment onto the n-Tm_2O_3/ITO electrode whereas the secondary and tertiary structures of ChOx play important roles for increased availability of active sites. Thus the ChEt–ChOx/n-Tm_2O_3/ITO bioelectrode provides easier electron transfer due to increased active sites for electrical contact between the electrode and the redox label in solution, resulting in improved diffusion of ferricyanide molecules towards the electrode surface.[49,50]

Table 1 Values of interfacial kinetic parameters of the corresponding electrodes during the surface-controlled process

Electrode	Anodic peak current (I_p, A)	Charge transfer rate constant (K_s, s^{-1})	Diffusion co-efficient (D, $cm^2\ s^{-1}$)	Average surface concentration (γ, mol cm^{-2})
n-Tm_2O_3/ITO	2.71×10^{-4}	2.076	2.17×10^{-5}	3.88×10^{-11}
ChEt–ChOx/n-Tm_2O_3/ITO	3.28×10^{-4}	1.315	3.19×10^{-5}	4.69×10^{-11}

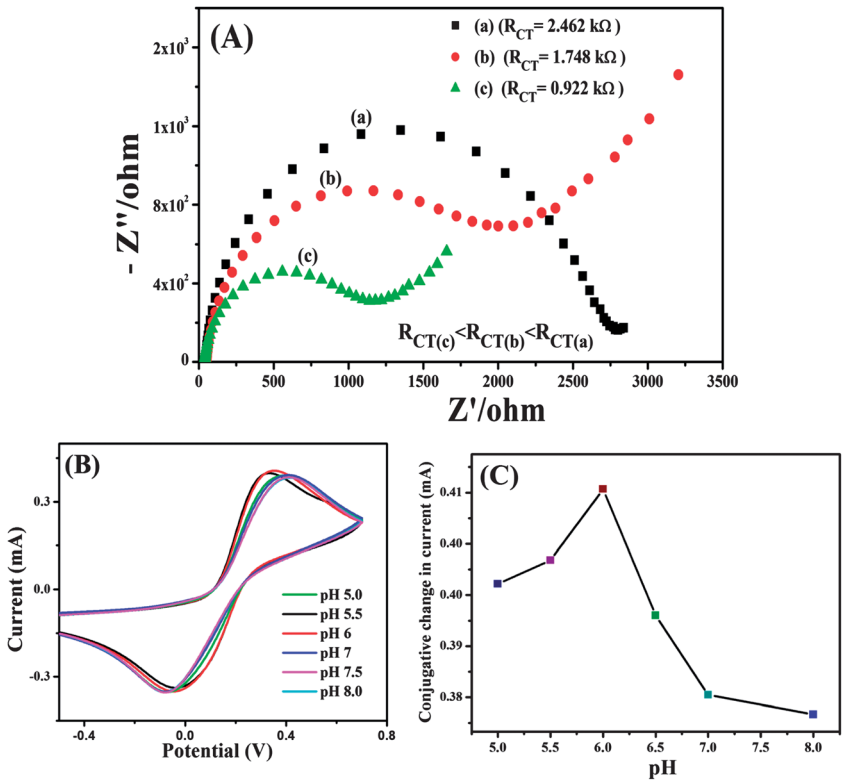

Fig. 5 (A) EIS of the bare ITO electrode (a), the n-Tm_2O_3/ITO electrode (b) and the ChEt–ChOx/n-Tm_2O_3/ITO bioelectrode (c). (B) CV studies of the ChEt–ChOx/n-Tm_2O_3/ITO bioelectrode as a function of pH (ranging from 5.0–8.0) in phosphate buffer containing $[Fe(CN)_6]^{3-/4-}$. (C) Change in current as a function of pH of the PBS for the ChEt–ChOx/n-Tm_2O_3/ITO bioelectrode.

Optimization of experimental variables

The effect of solution pH (5.0 to 8.0) on the electrochemical behaviour of the ChEt–ChOx/n-Tm_2O_3/ITO bioelectrode is measured by the CV technique in PBS (50 mM, 0.9% NaCl) containing $[Fe(CN)_6]^{3-/4-}$ (5 mM) at a 30 mV s^{-1} scan rate (Fig. 5B). It can be seen that the oxidation peak current increases from pH 5.0 to 6.0 and the peak potential shifts towards lower potential and the highest magnitude of current is obtained at pH 6.0 (Fig. 5C). When pH further increases from 6 to 8, the oxidation peak current decreases gradually and the potential peak shifts to the higher value. The limited electron transport between the medium and the electrode may lead to a decrease in the electrochemical signal at higher pH (~8.0). These changes in the peak current may arise due to a decrease in concentration of the positively charged moieties (Tm^{+3}) present at the matrix as the pH of PBS approaches its isoelectric point (IEP); this could result in decreased interaction between redox ions $[Fe(CN)_6]^{3-/4-}$ and the n-Tm_2O_3/ITO surface. Thus pH 6 is selected as the optimum pH for further experiments for cholesterol detection and at this pH, enzymes retain their natural structures in the interface and do not denature. The electrochemical measurements have been conducted in triplicate under identical conditions, and the measurements are reproducible. Moreover, it appears that higher pH is responsible for desorption of the enzyme, and the current response decreases by 25% at pH < 8.0. The optimized working potential of 0.3 V has been used (see Fig. S4 in the ESI†). Further optimization of experimental conditions such as the amount of ChOx and ChEt is maintained in the ratio of 1 : 1 to obtain the maximum amperometric current. The optimum amount of enzyme (ChEt + ChOx) solution used for immobilization onto the surface of the n-Tm_2O_3/ITO electrode is 15 μL (see Fig. S5 in the ESI†). The smaller amount of enzyme gives lower sensitivity, possibly due to decreased loading of enzyme molecules. Moreover, when the amount of the enzymes is too large, the electrode shows very high electrochemical impedance, resulting in decreased sensitivity and increased response time. The ChOx/ChEt loading has been found to affect amperometric response

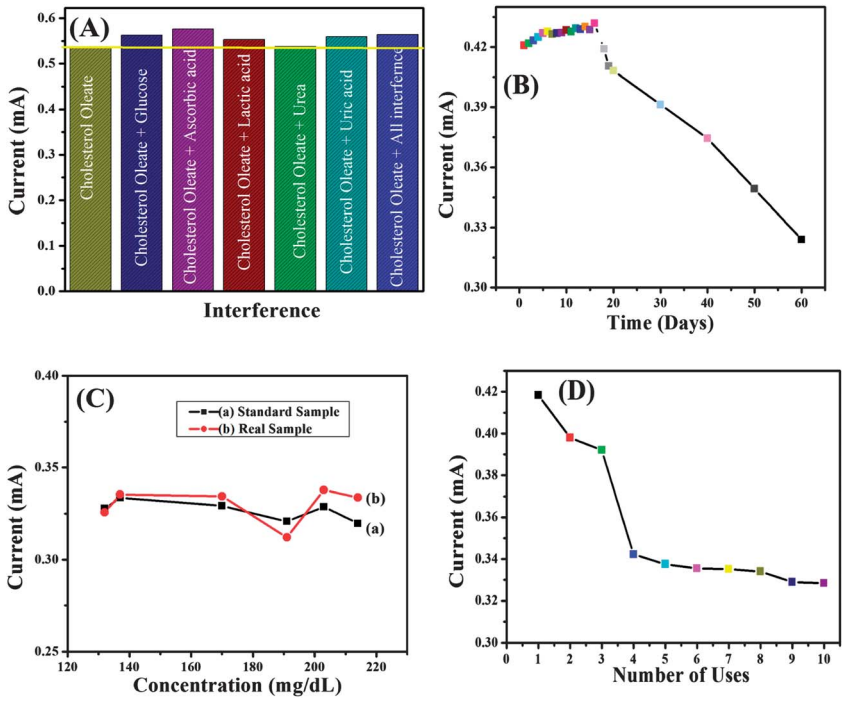

Fig. 6 (A) The bar graph shows the effect of different interferents on the electrochemical response of the ChEt–ChOx/n-Tm_2O_3/ITO bioelectrode. (B) Shelf-life curve of the ChEt–ChOx/n-Tm_2O_3/ITO bioelectrode as a function of day. (C) Determination of the total cholesterol concentration: (a) prepared standard cholesterol oleate solution and (b) cholesterol concentration in real clinical serum samples. (D) Reusability of the ChEt–ChOx/n-Tm_2O_3/ITO bioelectrode for the estimation of total cholesterol in real samples.

of the biosensor at 100 mg dL^{-1} cholesterol oleate (see Fig. S6 in the ESI†). The maximum current is obtained at 2 mg mL^{-1} of enzyme (ChOx–ChEt) loading. Hence, 2 mg mL^{-1} of enzyme has been used to fabricate the desired biosensor.

Effect of interferents, response time, thermal stability, reproducibility and shelf-life of the fabricated ChEt–ChOx/n-Tm_2O_3/ITO bioelectrode

The effect of common interferents (see Fig. S7 in the ESI†) on the fabricated ChEt–ChOx/n-Tm_2O_3/ITO bioelectrode has been estimated by using the equation $(I_{ch} - I_{int})/I_{ch}$, where I_{ch} and I_{int} are the steady-state oxidation current recorded for PBS containing an equal amount (1 : 1) of cholesterol oleate (100 mg dL^{-1}) and normal physiological concentration and 10 times more than normal physiological concentration of interferents such as glucose (5.0 & 50 mM), ascorbic acid (0.05 & 0.5 mM), lactic acid (0.5 & 5.0 mM), urea (1.0 & 10.0 mM), uric acid (0.1 & 1.0 mM) and a mixture of all interferents and comparing these with the control sample (cholesterol oleate, 100 mg dL^{-1}) using CV measurements at a 30 mV s^{-1} scan rate. The value of the oxidation current response decreases by 4.82%, 7.39%, 3.11%, 0.18%, 4.27% and 5.07% on addition of glucose, ascorbic acid, lactic acid, urea, uric acid and a mixture of all interferents, respectively (Fig. 6A) at normal physiological concentration of the interferents. In addition, the value of the oxidation peak current response decreases by 2.45%, 0.49%, 5.88%, 0.18%, 4.66% and 3.68% on addition of glucose, ascorbic acid, lactic acid, urea, uric acid and a mixture of all interferents, respectively {see Fig. S7(ii & iii) in the ESI†} in 10 times more than physiological concentration of the interference.

The response time of the ChEt–ChOx/n-Tm_2O_3/ITO bioelectrode (see Fig. S8 in the ESI†) has been measured *via* amperometric current response studies of the bioelectrode at an incubation period of 5 to 60 s. The magnitude of current increases initially (5 to 40 s) and the sensor achieves 95% of the steady-state current in less than 40 s. After 40 s, the current becomes almost constant indicating that 40 s is the response time of the ChEt–ChOx/n-Tm_2O_3/ITO bioelectrode.

The effect of temperature on reaction kinetics of the immobilized enzyme of the fabricated ChEt–ChOx/n-Tm_2O_3/ITO bioelectrode has been investigated at temperatures ranging from 15 to 60 °C (see Fig. S9 in the ESI†). The result shows that the fabricated bioelectrode is thermally stable up to 50 °C.

The shelf-life of the ChEt–ChOx/n-Tm_2O_3/ITO bioelectrode (Fig. 6B) has been investigated by measuring the amperometric current response in the presence of 100 mg dL^{-1} standard cholesterol oleate solution in PBS at a regular interval of 1 day up to 20 days and then after a gap of 10 days. It can be seen that the fabricated bioelectrode retains its enzyme activity up to 97% after 20 days, 93% after 30 days, 89% after 40 days and falls to 77% after 60 days when stored under refrigerated conditions (4 °C). The loss of sensitivity can be attributed to the decay of enzyme activity and leakage of the enzymes from the matrix. To evaluate applicability (Fig. 6C) and reusability (Fig. 6D) of this cholesterol biosensor in clinical analysis, efforts have been made to estimate the total cholesterol concentration using the

fabricated ChEt–ChOx/n-Tm_2O_3/ITO bioelectrode in real clinical serum samples obtained from a clinic located in New Delhi.

Discussion

The TEM studies of n-Tm_2O_3 show a rod-like structure with a diameter of 70 nm and with a dense wrinkled rough surface that is helpful for the immobilization of enzymes (Fig. 2B & C). The surface morphology of the n-Tm_2O_3 and the ChEt and ChOx immobilized electrode has been examined by SEM. The spindle and fibril elongated morphology of the n-Tm_2O_3 film changes to a homogeneous globular porous morphology due to ionic interactions between n-Tm_2O_3 and biomolecules, indicating immobilization of enzymes [Fig. 3B & C]. Moreover, the fibrous network of the n-Tm_2O_3 film provides increased surface area for immobilization of biomolecules resulting in enhanced enzyme loading. The presence of characteristic peaks at 1580 cm^{-1} and 1181 cm^{-1} can be assigned to C–O stretching due to amide bands in protein, revealing immobilization onto the ChEt–ChOx/n-Tm_2O_3/ITO bioelectrode *via* electrostatic interactions. The current response for different concentration of cholesterol oleate has been measured under optimized experimental conditions (Fig. 5B), working potential (see Fig. S4 in the ESI†) and amount of enzyme (ChOx + ChEt, 15 μL) has been used for the immobilization onto the surface of the n-Tm_2O_3/ITO electrode and the maximum current is obtained at 2 mg mL^{-1} of enzyme loading (see Fig. S5 in the ESI†). The electrochemical measurements conducted on a three-electrode system with ChEt–ChOx/n-Tm_2O_3/ITO as the working bioelectrode, a platinum (Pt) wire as the counter electrode and saturated Ag/AgCl as a reference electrode in phosphate buffer saline (PBS, 50 mM, pH 6.0 and 0.9% NaCl) containing 5 mM $[Fe(CN)_6]^{3-/4-}$ as a mediator and the signal transducer is in the form of amperometric current. The oxidative and reductive currents are found to increase on addition of cholesterol oleate solution to obtain the calibration curve (0–400 mg dL^{-1}) *i.e.* cholesterol oleate concentration *vs.* current. The same set-up has been used for estimation of cholesterol in real samples. The amperometric response studies (Fig. 7A) of the ChEt–ChOx/n-Tm_2O_3/ITO bioelectrode show oxidation peaks obtained at about 0.43 V corresponding to the oxidation of H_2O_2 arising due to the enzymatic reaction between enzymes (ChEt–ChOx) and cholesterol oleate. The magnified image of the sensing response of the selected area is shown in the inset of Fig. 7A. The increase in magnitude of the current with increase in cholesterol oleate concentration (0–400 mg dL^{-1}) is attributed to the increase in H_2O_2 concentration by enzymatic reaction, which on oxidation generates electrons and contributes to the increase in current. This may be due to a well-aligned cubic crystal structure of n-Tm_2O_3 nanoparticles. This interfacial network acts as a decent acceptor of electrons, which are generated during the re-oxidation of enzymes and are transferred to the electrode *via* Tm(II)/Tm(III) redox coupling, resulting in increased amperometric response. The peak potential shifts to less anodic values, from 0.43–0.41 V, with increasing cholesterol concentration (8–400 mg dL^{-1}). This behaviour may be ascribed to the

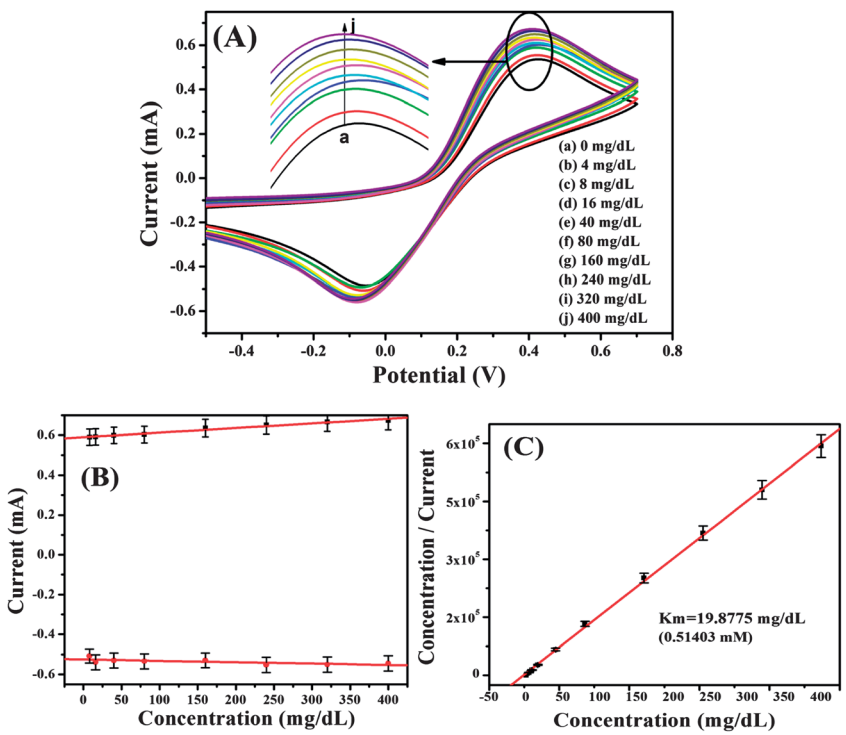

Fig. 7 (A) Electrochemical response of the ChEt–ChOx/n-Tm_2O_3/ITO bioelectrode with respect to the cholesterol oleate concentration (0–400 mg dL^{-1}) in phosphate buffer containing $[Fe(CN)_6]^{3-/4-}$ at a scan rate of 30 mV s^{-1}. (B) Calibration curve of the ChEt–ChOx/n-Tm_2O_3/ITO bioelectrode and the variation in current as a function of cholesterol oleate concentration (0–400 mg dL^{-1}) in phosphate buffer containing $[Fe(CN)_6]^{3-/4-}$ at a scan rate of 30 mV s^{-1}. (C) Hanes plot, which plots the substrate concentration (*X*-axis) and substrate concentration/current (*Y*-axis).

availability of more active sites of enzymes associated with a higher cholesterol concentration and in turn to a lower potential value. The corresponding calibration curve (Fig. 7B) shows that the magnitude of the oxidation peak current increases almost linearly with increasing cholesterol oleate concentration and saturates at higher concentration of cholesterol oleate. However, under optimized conditions, the enzyme immobilized ChEt–ChOx/n-Tm_2O_3/ITO bioelectrode shows a broad linear range to analyte in the concentration range from 8 to 400 mg dL^{-1} which is relatively better than that reported in the literature.[51,52] The sensitivity of the fabricated bioelectrode calculated from the slope of the curve is estimated to be 0.925 μA (mg per dL $cm^{-2})^{-1}$ which is found to be better than the reported value.[22,30,47,51–53] The standard deviation and detection limit of the bioelectrode are found to be 6.097 μA and 19.78 mg $(dL\ cm^2)^{-1}$, respectively. Since the desired total plasma cholesterol for an individual is less than 5.2 mM (200 mg dL^{-1}), with a high level being considered as greater than 6.2 mM (240 mg dL^{-1}), the fabricated biosensor covers a wide range of cholesterol concentration, promising for the clinical diagnostics of total cholesterol. The electrochemical reactions that occur during the detection of total cholesterol in the presence of ChEt and ChOx are shown in eqn (5)–(7).

$$\text{Cholesterol oleate} + H_2O \xrightarrow{\text{ChEt}} \text{cholesterol} + \text{fatty acid} + \text{ChEt} \quad (5)$$

$$\text{Cholesterol} + O_2 \xrightarrow{\text{ChOx}} \text{cholest-4en-3one} + H_2O_2 \quad (6)$$

$$H_2O_2 \xrightarrow[0.43\ V]{\text{electrochemical oxidation}} 2H^+ + O_2 + 2e^- \quad (7)$$

The enzyme–substrate kinetic parameter (Michaelis–Menten constant, K_m) of the ChEt–ChOx/n-Tm_2O_3/ITO bioelectrode has been calculated using the Hanes plot *i.e.* graph between [substrate concentrations] and [substrate concentration/current] (Fig. 7C) and is found to be 19.88 mg dL^{-1} (0.51 mM) which is much lower than the reported value.[2,22,52,53] When the enzymes are immobilized on the surface of the n-Tm_2O_3/ITO film, a higher concentration of substrate is required to overcome the effects of the nanostructured film. Therefore, the K_m value is higher for the immobilized enzyme when compared to that of the free enzyme. The values of enzyme kinetic properties are known to depend on the enzyme conformation and its nano-environment in the interface, stearic effects, bulk and diffusion effects.[54,55] The observed small K_m value indicates increased affinity of the ChEt–ChOx/n-Tm_2O_3/ITO bioelectrode for the substrate, which is attributed to the favourable conformation of bienzyme (ChEt–ChOx) and its more efficient loading onto the n-Tm_2O_3/ITO electrode surface. It appears that the n-Tm_2O_3 film provides increased activity of the immobilized biomolecules perhaps due to their improved conformation and orientation, leading to enhanced interaction and communication between the enzyme and the substrate molecules at the interface. Additionally, the cholesterol biosensor based on the n-Tm_2O_3 modified interface exhibits good selectively and stability of up to 70 days. Table 2 summarises results of studies using the ChEt–ChOx/n-Tm_2O_3/ITO bioelectrode including those reported in the literature.[2,22,23,30,38,47,51–53,56–60]

We have investigated the electrochemical performance of two different nanorods (sample A & sample B) having dimensions as length ~800 nm, diameter ~85 nm (Fig. S10†) and length 610 nm and diameter as 70 nm (Fig. 1). Fig S11† shows the variation of the oxidation current of the n-Tm_2O_3 (sample A)/ITO electrode and n-Tm_2O_3 (sample B)/ITO electrode. It can be seen that the n-Tm_2O_3 (sample B)/ITO electrode with smaller dimensions exhibits improved current response indicating that the size of n-Tm_2O_3 nanorods plays a significant role in the response of the n-Tm_2O_3/ITO based cholesterol sensor.

Table 2 Characteristics of the ChEt–ChOx/n-Tm_2O_3/ITO cholesterol sensor and other metal oxide nanoparticles or metal oxide mixed biopolymer based cholesterol biosensor reported in the literature, along with their important parameters

SN	Material	Linearity (mg dL^{-1})	Detection limit (mg dL^{-1})	Sensitivity (μA mg^{-1} dL^{-1})	K_m value (mM)	Response time (second)	Shelf-life (days)	Ref.
1	ChOx/NS–CeO_2/ITO	9.67–39.64	9.67	0.155	2.06	15	—	2
2	ChOx/nano-NiO–CHIT/ITO	10–400	43.4	0.808	0.66	15	63	22
3	ChEt–ChOx/MWCNT/SiO_2–CHIT/ITO	10–500	0.634	0.098	0.052	10	63	23
4	ChOx/$NiFe_2O_4$/CuO/FeO–CH/ITO	5–500	31.3	0.043	0.21	10	90	30
5	ChOx/nano-ZnO–CHIT/ITO	05–300	5	1.41×10^{-10}	0.22	15	85	38
6	*N*-(2-Aminoethyl)-3-aminopropyl-trimethoxysilane SAM	50–500	25	0.449	1.5	—	70	47
7	(3-Glycidoxypropyl) trimethoxysilane SAM	100–400	—	0.351	0.43	40	70	51
8	PANI/ITO	25–400	25	0.776	0.62	—	77	52
9	Polyaniline	50–500	25	0.042	1.94	240	42	53
10	ChEt–ChOx/Ufm-Cu_2O–CS/ITO	10–450	15.9	0.895	0.979	<5	60	56
11	ChOx/nano-ZnO/ITO	10–300	0.5	0.059	0.223	10	56	57
12	ChOx/CoO(NPs)/GC	0.16–1.93	0.16	0.001	0.49	15	—	58
13	ChEt–ChOx/$NiFe_2O_4$–CH/ITO	5–400	24.46	1.73	0.18	15	90	59
14	ChOx/CS–SnO_2/ITO	10–400	5	34.7	3.8	5	42	63
15	ChEt–ChOx/n-Tm_2O_3/ITO	8–400	19.78	0.924	0.514	40	60	Present work

Table 3 Determination of cholesterol in serum samples

S.no	Cholesterol concentration (mg dL^{-1})	Values of current obtained with serum samples (mA)	Values of current obtained for pure cholesterol oleate samples (mA)	% RSD	Spectrophotometry content (mg dL^{-1})
1	132	0.326	0.328	0.65	132 ± 1
2	137	0.336	0.334	0.55	137 ± 0.5
3	170	0.334	0.329	1.57	170 ± 1
4	191	0.312	0.321	2.71	191 ± 0.5
5	203	0.338	0.329	2.76	203 ± 2

Application of the ChEt–ChOx/n-Tm_2O_3/ITO bioelectrode to serum samples

Cholesterol is found in biological media in the free form (about 30% of the total content) or as cholesterol ester (approximately 70% of the total content).[23,61] The practical usage of a biosensor is assessed by the determination of the total cholesterol concentration in human serum, since the concentrations of free cholesterol and esterified cholesterol in human serum range between 49 and 80 mg dL^{-1} and between 81 and 172 mg dL^{-1}, respectively.[62] The concentration of total cholesterol in a real serum sample has been determined using the following procedure: 15 mL of PBS (50 mM, pH 6.0 and 0.9% NaCl, containing 5 mM $[Fe(CN)_6]^{3-/4-}$) has been used as the electrolyte solution. The assay for free cholesterol and esterified cholesterol in serum has been carried out similar to that for immobilized enzyme except that the substrate is replaced with pre-treated 10 μL serum samples diluted with 2.0 mL phosphate buffer. This dilution of the serum sample is necessary in order to obtain measurement accuracy due to the saturation behaviours of current response at higher concentration. The amperometric current response has been measured both in serum and the standard sample in the presence of electrolyte under optimized experimental conditions. It can be seen (Fig. 6C) that the magnitude of current obtained with serum samples (132, 137, 170, 191, 203 and 214 mg dL^{-1}) and from the standard cholesterol oleate solution (identical to the concentrations of the serum samples) is in reasonable agreement. To validate the accuracy of the fabricated cholesterol biosensor, the concentration of total cholesterol in serum samples determined by the fabricated biosensor has been compared with the value measured by the commercial spectrophotometric method in the laboratory (Table 3). The results obtained suggest that the concentration of total cholesterol in human serum samples determined by using the techniques developed in the present study is in acceptable agreement with the results determined using spectrophotometric methods in a clinic located in New Delhi. Thus, we may utilize the fabricated ChEt–ChOx/n-Tm_2O_3/ITO bioelectrode as a new electrochemical rare earth metal oxide interface for the determination of cholesterol in clinical diagnostics. The reusability of the fabricated ChEt–ChOx/n-Tm_2O_3/ITO bioelectrode for the estimation of cholesterol in the real sample (132 mg dL^{-1}) has been determined. The results indicate that the bioelectrode can be reused up to 10 cycles with a loss of 22% current response (Fig. 6D). Further, this bioelectrode has been used in clinical applications to estimate total cholesterol levels with negligible interference (3%) from analytes present in human serum samples.

Conclusions

In summary, a cholesterol biosensor has been fabricated by immobilizing ChOx and ChEt on the surface of Tm_2O_3 nanorods using an electrochemical technique. The Tm_2O_3 nanorods modified interface significantly contributes to improved electron transfer kinetics, electro-active surface area, diffusion coefficient and surface concentration. The ChEt–ChOx/n-Tm_2O_3/ITO bioelectrode shows a sensitivity of 0.9245 μA (mg per dL $cm^{-2})^{-1}$, broad linear range of 8–400 mg dL^{-1} for total cholesterol, standard deviation of 6.0965 μA, detection limit of 19.78 mg (dL $cm^2)^{-1}$ and response time of 40 s. The superior performance of the ChEt–ChOx/n-Tm_2O_3 interface based biosensor is combined with long-term stability, reproducibility and excellent specificity to cholesterol in the presence of common interferents. The ChEt–ChOx/n-Tm_2O_3/ITO bioelectrode is a potential platform for determination of total cholesterol in human serum samples. In view of the excellent characteristics of this ChEt–ChOx/n-Tm_2O_3/ITO interface for a total cholesterol biosensor, efforts should be made to involve international agencies for speedy commercialization of this bioelectrode. The enzyme modified n-Tm_2O_3 electrode interface offers an efficient strategy and a new promising platform for biomedical application of rare earth metal oxide materials towards development of nanobiosensors, nanobiofuel cells and other bioelectronics devices. Efforts should be made to ascertain the effect of the size of the Tm_2O_3 nanorods on the electrochemical performance of enzyme (ChOx and ChEt) immobilized Tm_2O_3. The results of these studies open a new perspective in rare earth metal oxide for biomedical applications.

Experimental section

Materials

The reagents used for the synthesis of thulium(III) oxide nanorods are as follows. Thulium(III) nitrate pentahydrate (325996-5G) was purchased from Sigma-Aldrich (USA). The sodium hydroxide (NaOH) pellets were procured from MERCK (New Delhi, India). Cholesterol oxidase (C7149, EC 1.1.36 from *Pseudomonas fluorescens* with a specific activity of 26.4 U mg^{-1}), cholesterol esterase (C1403, EC 232.808.6 from *Pseudomonas fluorescens* with a specific activity of 13.13 U mg^{-1}), horseradish peroxidise (HRP, P8415, 250-330 U mg^{-1}), *O*-dianisidine (D9143, 1%) dye, cholesterol oleate (C9253, $C_{45}H_{78}O_2$) and Brij L23 solution (B4184) were purchased from Sigma-Aldrich (USA). The stock solutions of ChOx and ChEt (2 mg mL^{-1}) and HRP

(1 mg mL^{-1}) were prepared in phosphate buffer (50 mM, pH 7.0) prior to use. Cholesterol oleate (400 mg dL^{-1}) solution was prepared by dissolving it (40 mg) in 1% Brij L23 solution as a surfactant by heating and gentle stirring. The *O*-dianisidine (1%) solution was freshly prepared (3 mg mL^{-1}) in de-ionized water.

Preparation of Tm_2O_3 nanorods

The thulium oxide (Tm_2O_3) nanorods were prepared using the hydrothermal homogeneous method. In brief, first we prepared a solution of 200 mM thulium nitrate [$Tm(NO_3)_3$, $5H_2O$] in 20 mL of deionized water and later another solution containing 1 M of sodium hydroxide (NaOH) in 100 mL of deionized water was separately prepared. Then, the NaOH solution was added dropwise into the thulium nitrate solution with constant stirring (pH ~12) to obtain a turbid white precipitate at room temperature (25 °C). The resulting solution was transferred to a 50 mL Teflon-lined stainless steel autoclave and maintained at 180 °C for 15 h after which it was allowed to cool to room temperature (25 °C). The resulting pale white precipitate was filtered and washed several times with de-ionized water and absolute ethanol to eliminate the presence of the ionic remnants. The precipitate was then dried at 80 °C for 6 h and calcined at 500 °C for 3 h to obtain n-Tm_2O_3 nanorods.

Electrophoretic deposition of the n-Tm_2O_3/ITO film

Electrophoretic deposition (EPD) was carried out using a DC battery (BioRad, model 200/2.0) as the power supply. 50 mg of n-Tm_2O_3 nanorods was dispersed in 5 mL of double distilled water and the solution was ultra-sonicated for 30 min. A platinum foil (1 cm × 2 cm) was used as an anode and a hydrolyzed ITO-coated glass plate as a cathode. The two electrodes, placed parallel to each other with separation of 1 cm, were dipped in n-Tm_2O_3 colloidal suspension. Film deposition was executed onto an ITO plate (0.25 cm^2) at 25 mV for 40 s and then removed from the suspension followed by washing with de-ionized water to remove any unbound particles.

Immobilization of ChEt and ChOx onto the n-Tm_2O_3/ITO electrode

The immobilization of ChOx and ChEt (1 : 1) was carried out by uniformly spreading 15 μL of optimal enzyme solution onto the n-Tm_2O_3/ITO electrode surface to obtain the maximum current response. The ChEt–ChOx/n-Tm_2O_3/ITO bioelectrode was placed undisturbed overnight in a humid chamber. Finally, the dry ChEt–ChOx/n-Tm_2O_3/ITO bioelectrode was immersed in 50 mM phosphate buffer saline (PBS) (pH 7.0, 0.9% NaCl) in order to remove any unbound enzymes from the electrode surface. The ChEt–ChOx/n-Tm_2O_3/ITO bioelectrode was stored under refrigerated conditions when not in use.

Photometric enzyme activity

The apparent enzyme activity (U cm^{-2}) is defined as one unit of enzyme activity that results in conversion of 1 μmol of cholesterol into cholest-4-ene-3-one per minute.[63] The experimental details are given in the ESI.† The apparent enzyme activity has been calculated to be 0.865 U cm^{-2} indicating that 0.865 (54.62%) units of enzyme per cm^2 actively participated in the enzymatic reaction.

Characterization and measurements

The characterization of the Tm_2O_3 nanorods has been accomplished using X-ray diffraction (XRD) and a Rigaku D/Max 2200 diffractometer with CuKα radiation at $\lambda = 1.540$ Å. FT-IR spectra of the electrodes were recorded using an FT-IR spectrophotometer (PerkinElmer, Spectrum BX II). The UV-visible spectroscopic studies were conducted using a UV/VIS/NIR spectrometer (PerkinElmer, Lamda 950). The transmission electron microscopy (TEM) studies were carried out with a JEOL JEM-2200 FS (Japan). The surface morphological studies of Tm_2O_3 nanorods were investigated using a scanning electron microscope (LEO-440). X-ray photoelectron spectroscopy (XPS) studies were performed using an Axis-Nova, Kratos Analytical Ltd., Manchester, UK. The cyclic voltammetry (CV), electrochemical impedance spectroscopy (EIS) and amperometric measurements were conducted using an Autolab Potentiostat/Galvanostat (Eco Chemie, The Netherlands).

Author contributions

J.S., A.R. and B.D.M. wrote the manuscript text. J.S. and A.R. designed and carried out the experiments and analysed the data. M.S. performed the XRD, HRTEM, and SEM characterization and structural analysis. D.W.L., S.H.L. and B.D.M. supervised the studies and discussed the results. All the authors have reviewed the manuscript and have participated in discussions of the results of this research.

Notes

The authors declare no competing financial interest.

Acknowledgements

This study was supported by the BK 2 plus project through the National Research Foundation (NRF) funded by the Ministry of Education, Science, and Technology (MEST) Republic of Korea. J.S. acknowledges the Department of Science & Technology, Govt of India for awarding the DST-INSPIRE Fellowship [IFA-13 CH-105]2013 and DST Young Scientist award (CS-393/2012), and the financial support received under the Department of Science & Technology project [DST/TSG/ME2001/18, Govt of India], the in-house project (OLP-070632D) and the Indian Council of Medical Research project (ICMR/RHN/ADHOC/5/2012-2013) is gratefully acknowledged. A.R. is thankful to the Indian Council of Medical Research (ICMR) for the award of Project Associateship. B.D.M. thanks the Ministry of Education, Science and Technology (R32-20026) of Korea for the opportunity provided during his visit to the Chungnam National University as visiting professor under the World Class University project during March–July 2013.

References

1 Y. M. Shi, P. Wu, P. Du and C. X. Cai, *Acta Phys.–Chim. Sin.*, 2006, **22**, 1227–1232.
2 A. A. Ansari, A. Kaushik, P. R. Solanki and B. D. Malhotra, *Electrochem. Commun.*, 2008, **10**, 1246–1249.
3 P. R. Solanki, A. Kaushik, V. V. Agrawal and B. D. Malhotra, *NPG Asia Mater.*, 2011, **3**, 17–24.
4 X. L. Xiao, Q. F. Luan, X. Yao and K. B. Zhou, *Biosens. Bioelectron.*, 2009, **24**, 2447–2451.
5 M.-H. Wu, Y.-F. Lee, C.-W. Lin, S.-W. Tsai, H.-Y. Wang and T.-M. Pan, *J. Mater. Chem.*, 2011, **21**, 539–547.
6 L. Yu and J. Xi, *Int. J. Hydrogen Energy*, 2012, **37**, 15938–15947.
7 J. J. Wang, Z. B. Fang, T. Ji, W. Y. Ren, Y. Y. Zhu and G. He, *Appl. Surf. Sci.*, 2012, **258**, 6107–6110.
8 L. Eyring, in *The Handbook on the Physics and Chemistry of Rare Earths*, ed. K. A. Gschneider, Jr and L. Eyring, North Holland, Amsterdam, 1979.
9 L. C. Chandola and P. P. Khanna, *J. Radioanal. Nucl. Chem.*, 1988, **121**, 53–59.
10 R. Lisiecki, B. Macalik, G. Dominiak-Dzik, P. Solarz, B. Nowak, R. W. Romanowdki, J. K. Jabczynski and T. Lukasiewicz, *Appl. Phys. B: Lasers Opt.*, 2008, **90**, 477–483.
11 Y. Castrillejo, P. Fernánda, M. R. Bergmejo, E. Barrado and A. M. Martínez, *Electrochim. Acta*, 2009, **54**, 6212–6222.
12 G. F. Wang, W. P. Qin, J. S. Zhang, J. S. Zhang, Y. Wang, C. Y. Cao, L. L. Wang, G. D. Wei, P. F. Zhu and R. Kim, *J. Phys. Chem. C*, 2008, **112**, 12161–12167.
13 S. J. Xia, J. Zhuo, X. W. Sun, B. M. Han, Y. Shao and Y. N. Zhang, *Eur. Urol.*, 2008, **53**, 382–390.
14 T. M. Pan, C. D. Lee and M. H. Wu, *J. Phys. Chem. C*, 2009, **113**, 21937–21940.
15 R. O. Connor, V. S. Chang, L. Pantisano, L. A. Ragnarsson, M. Aoulaiche, B. O. Sullivan and G. Groeseneken, *Appl. Phys. Lett.*, 2008, **93**, 053506.
16 Q. L. Sheng, H. Yu and J. B. Zheng, *J. Electroanal. Chem.*, 2007, **606**, 39–46.
17 Z. Meng, J. Zheng, Q. Sheng and X. Zheng, *Anal. Chim. Acta*, 2011, **689**, 47–51.
18 Y. Li, Y. Gao, Y. Zhou, Y. Liu and J. Liu, *J. Electroanal. Chem.*, 2010, **642**, 1–5.
19 A. A. Tolstopyatova and A. A. Balandin, *Russ. Chem. Bull.*, 1965, **14**, 1923–1928.
20 Y. Li, Y. Gao, Y. Liu, Y. Zhou and J. Liu, *J. Inn. Mong. Norm. Univ., Nat. Sci. Ed.*, 2010, **29**, 254–259.
21 U. Saxena, M. Chakraborty and P. Goswami, *Biosens. Bioelectron.*, 2011, **26**, 3037–3043.
22 J. Singh, P. Kalita, M. K. Singh and B. D. Malhotra, *Appl. Phys. Lett.*, 2011, **98**, 123702.
23 P. R. Solanki, A. Kaushik, A. A. Ansari, A. Tiwari and B. D. Malhotra, *Sens. Actuators, B*, 2009, **137**, 727–735.
24 W. Richmond, *Clin. Chem.*, 1973, **19**, 1350–1356.
25 S. P. Martin, D. J. Lamb, J. M. Lynch and S. M. Reddy, *Anal. Chim. Acta*, 2003, **487**, 91–100.
26 A. K. Basu, P. Chattopadhyay, U. Roychoudhuri and R. Chakraborty, *Biochemistry*, 2007, **70**, 375–379.
27 R. Manjunatha, S. G. Shivappa, J. S. Melo, S. F. D'Souza and T. V. Venkatesh, *Talanta*, 2012, **99**, 302–309.
28 A. L. Crumbliss, J. G. Stonehuerner and R. W. Henkens, *Biochemistry*, 1993, **8**, 331–337.
29 F. Cheng, H. Jishan and C. Zhencheng, *Sens. Actuators, B*, 2011, **155**, 545–550.
30 J. Singh, M. Srivastava, P. Kalita and B. D. Malhotra, *Process Biochem.*, 2012, **47**, 2189–2198.
31 S. A. Ansari and Q. Husain, *Biotechnol. Adv.*, 2012, **30**, 512–523.
32 C. C. Lin and M. C. Yang, *Biomaterials*, 2003, **24**, 549–557.
33 J. P. Liu, C. X. Guo, C. M. Li, Y. Y. Li, Q. B. Chi, X. T. Huang, L. Liao and T. Yu, *Electrochem. Commun.*, 2009, **11**, 202–205.
34 K. J. Byrappa, *J. Ceram. Soc. Jpn.*, 2009, **117**, 236–244.
35 H. Liu, D. Chen, L. Yang, X. Ren and F. T. J. Ren, *Nanotechnology*, 2010, **21**, 185504–185510.
36 R. Ahmad, N. Tripathy and Y.-B. Hahn, *Biosens. Bioelectron.*, 2013, **45**, 281–286.
37 A. R. Boccaccini, S. Keim, R. Ma, Y. Li and I. Zhitomirsky, *J. R. Soc., Interface*, 2010, **7**, S581–S613.
38 S. Srivastava, V. Kumar, Md A. Ali, P. R. Solanki, A. Srivastava, G. Sumana, P. S. Saxena, A. G. Joshid and B. D. Malhotra, *Nanoscale*, 2013, **5**, 3043–3051.
39 G. J. Zhou, G. Wang, J. J. Xu and H. Y. Chen, *Sens. Actuators B*, 2002, **81**, 334.
40 S. Singh, R. Singhal and B. D. Malhotra, *Anal. Chim. Acta*, 2007, **58**, 335–343.
41 J. Singh, M. Srivastava, A. Roychoudhury, D. W. Lee, S. H. Lee and B. D. Malhotra, *J. Alloys Compd.*, 2013, **578**, 405–412.
42 E. Laviron, *J. Electroanal. Chem. Interfacial Electrochem.*, 1979, **101**, 19–28.
43 J. Singh, A. Roychoudhury, M. Srivastava, P. R. Solanki, D. W. Lee, S. H. Lee and B. D. Malhotra, *J. Mater. Chem. B*, 2013, **1**, 4493–4503.
44 A. Sharma, G. Sumana, S. Sapra and B. D. Malhotra, *Langmuir*, 2013, **29**, 8753–8762.
45 S. K. Yadav, J. Singh, V. V. Agrawal and B. D. Malhotra, *Appl. Phys. Lett.*, 2012, **101**, 023703.
46 J. Shi, J. C. Claussen, E. S. McLamore, A. U. Haque, D. Jaroch, A. R. Diggs, P. Calvo-Marzal, J. L. Rickus and D. M. Porterfield, *Nanotechnology*, 2011, **22**, 355502.
47 S. K. Arya, A. K. Prusty, S. P. Singh, P. R. Solanki, M. K. Pandey, M. Datta and B. D. Malhotra, *Anal. Biochem.*, 2007, **363**, 210–218.
48 P. R. Solanki, S. K. Arya, Y. Nishimura, M. Iwamoto and B. D. Malhotra, *J. Biomed. Pharm. Eng.*, 2008, **2**(1), 7–13.
49 A. Kaushik, P. R. Solanki, K. Kaneto, C. G. Kim, S. Ahmad and B. D. Malhotra, *Electroanalysis*, 2010, **22**, 1045–1055.
50 H. L. Zhang, X. Z. Zou, G. S. Lai, D. Y. Han and F. Wang, *Electroanalysis*, 2007, **19**, 1869–1874.

51 S. Kumar, J. Singh, V. V. Agrawal, M. Ahmed and B. D. Malhotra, *Anal. Methods*, 2011, **3**, 2237–2245.
52 C. Dhand, S. P. Singh, S. K. Arya, M. Datta and B. D. Malhotra, *Anal. Chim. Acta*, 2007, **602**, 244–251.
53 S. Singh, P. R. Solanki, M. K. Pandey and B. D. Malhotra, *Sens. Actuators, B*, 2006, **115**, 531–534.
54 X. Yi, J. Huang-Xian and C. Hong-Yuan, *Anal. Biochem.*, 2000, **278**, 22–28.
55 J. F. Kennedy and C. A. White, *Handbook of Enzyme Biotechnology*, ed. Wiseman, John Wiley & Sons, New York, 2nd edn, 1985, pp. 147–201.
56 J. Singh, M. Srivastava, A. Roychoudhury, D. W. Lee, S. H. Lee and B. D. Malhotra, *J. Phys. Chem. B*, 2013, **117**, 141–152.
57 P. R. Solanki, A. Kaushik, A. A. Ansari and B. D. Malhotra, *Appl. Phys. Lett.*, 2009, **94**, 143901.
58 A. Salimi, R. Hallaj and S. Soltanian, *Electroanalysis*, 2009, **21**, 2693–2700.
59 J. Singh, A. Roychoudhury, M. Srivastava, V. Chaudhary, R. Prasanna, D. W. Lee, S. H. Lee and B. D. Malhotra, *J. Phys. Chem. C*, 2013, **117**, 8491–8502.
60 A. A. Ansari, A. Kaushik, P. R. Solanki and B. D. Malhotra, *Electroanalysis*, 2009, **21**, 965–972.
61 E. García, J. C. Vidal, M. T. Aramendìa and J. R. Castillo, *Electroanalysis*, 2004, **16**, 497–504.
62 T. Nakaminami, S. Ito, S. Kuwabata and H. Yoneyama, *Anal. Chem.*, 1999, **71**, 1068–1076.
63 R. Khan, A. Kaushik, P. R. Solanki, A. A. Ansari, M. K. Pandey and B. D. Malhotra, *Anal. Chim. Acta*, 2008, **616**, 207–213.

